J|A|C|S
ARTICLES
Published on Web 01/19/2007

Secondary Structures of Peptides and Proteins via NMR Chemical-Shielding Anisotropy (CSA) Parameters

Eszter Czinki,[⊥] Attila G. Császár,*[,⊥] Gábor Magyarfalvi,[⊥] Peter R. Schreiner,[‡] and Wesley D. Allen*[,§]

Contribution from the Laboratory of Molecular Spectroscopy, Institute of Chemistry, Eötvös University, H-1518 Budapest 112, P.O. Box 32, Hungary, Institute of Organic Chemistry, Justus-Liebig University, Heinrich-Buff-Ring 58, 35392 Giessen, Germany, and Center for Computational Chemistry, Department of Chemistry, University of Georgia, Athens, Georgia 30602

Received July 28, 2006; E-mail: wdallen@uga.edu; csaszar@chem.elte.hu

Abstract: Complete nuclear magnetic resonance (NMR) chemical-shielding tensors, $\boldsymbol{\sigma}$, have been computed at different levels of density-functional theory (DFT), within the gauge-including atomic orbital (GIAO) formalism, for the atoms of the peptide model For-L-Ala-NH_2 as a function of the backbone dihedral angles ϕ and ψ by employing a dense grid of 10°. A complete set of rigorously orthogonal symmetric tensor invariants, $\{\sigma_{iso}, \rho, \tau\}$, is introduced, where σ_{iso} is the usual isotropic chemical shielding, while the newly introduced ρ and τ parameters describe the magnitude and the orientation/shape of the chemical-shielding anisotropy (CSA), respectively. The set $\{\sigma_{iso}, \rho, \tau\}$ is unaffected by unitary transformations of the symmetric part of the shielding tensor. The mathematically and physically motivated $\{\rho, \tau\}$ anisotropy pair is easily connected to more traditional shielding anisotropy measures, like span (Ω) and skew (κ). The effectiveness of the different partitions of the CSA information in predicting conformations of peptides and proteins has been tested throughout the Ramachandran space by generating theoretical NMR anisotropy surfaces for our For-L-Ala-NH_2 model. The CSA surfaces, including $\Omega(\phi, \psi)$, $\kappa(\phi, \psi)$, $\rho(\phi, \psi)$, and $\tau(\phi, \psi)$ are highly structured. Individually, none of these surfaces is able to distinguish unequivocally between the α-helix and β-strand secondary structural types of proteins. However, two- and three-dimensional correlated plots, including Ω versus κ, ρ versus τ, and σ_{iso} versus ρ versus τ, especially for $^{13}C^{\alpha}$, have considerable promise in distinguishing among all four of the major secondary structural elements.

1. Introduction

One of the primary goals of proteomics is the determination of high-resolution three-dimensional structures of peptides and proteins. Detailed knowledge of protein structures on the atomic scale is regarded as one of the key factors in structure-guided drug development. It has been estimated[1] that development costs could be cut approximately in half if target protein structures were used at an early stage to generate leads in drug design.

Nuclear magnetic resonance (NMR) spectroscopy is a powerful tool for the structure determination of large molecules, particularly proteins in solution. The NMR technique is based on the sensitivity of magnetic properties, typically isotropic chemical shieldings (ICS), to the chemical environment of the nuclei. Structural information is readily extracted because NMR data primarily depend on the *local* chemical bonding environment, within a few Å of the nucleus under consideration. By means of elaborate, often multidimensional techniques, structures of hydrocarbons, sugars, and, in particular, peptides and proteins can be probed by various directional magnetization-transfer pulse sequences.[2−9]

Orientational averaging reduces the detailed information in the NMR chemical-shielding tensor to one, readily interpretable, ICS parameter.[10−13] For increasingly larger molecules with slow tumbling rates, however, the NMR resonances broaden and become harder to analyze. In principle, solid-state NMR techniques[14−16] can exploit this lack of orientational averaging

[⊥] Eötvös University.
[‡] Justus-Liebig University.
[§] University of Georgia.

(1) Stephens, R. C. *Nat. Struct. Mol. Biol.* **2004**, *11*, 93.
(2) Pines, A.; Gibby, M. G.; Wangh, J. S. *J. Chem. Phys.* **1973**, *59*, 569.
(3) Fesik, S. W.; Zuiderweg, E. R. P. *Q. Rev. Biophys.* **1990**, *23*, 97.
(4) Clore, G. M.; Gronenborn, A. M. *Prog. Nucl. Magn. Reson. Spectrosc.* **1991**, *23*, 43.
(5) Kay, L. E.; Keifer, P.; Saarinen, T. *J. Am. Chem. Soc.* **1992**, *114*, 10663.
(6) Bax, A.; Grzesiek, S. *Acc. Chem. Res.* **1993**, *26*, 131.
(7) Boisbouvier, J.; Brutscher, B.; Simorre, J. P.; Marion, D. *J. Biomol. NMR* **1999**, *14*, 241.
(8) Strohmeier, M.; Grant, D. M. *J. Am. Chem. Soc.* **2004**, *126*, 966.
(9) Wi, S.; Sun, H. H.; Oldfield, E.; Hong, M. *J. Am. Chem. Soc.* **2005**, *127*, 6451.
(10) Haeberlen, U. *Philos. Trans. R. Soc. London, Ser. A* **1981**, *299*, 497.
(11) Buckingham, A. D.; Malm, S. M. *Mol. Phys.* **1971**, *22*, 1127.
(12) Haeberlen, U. *High Resolution NMR In Solids*; Academic Press: New York, 1976.
(13) Andrew, E. R.; Eades, R. G. *Faraday Discuss.* **1962**, *34*, 38.
(14) Luca, S.; Heise, H.; Baldus, M. *Acc. Chem. Res.* **2003**, *36*, 858.
(15) Davis, J. H.; Auger, M. *Prog. Nucl. Magn. Reson. Spectrosc.* **1999**, *35*, 1.
(16) Warschawski, D. E.; Traikia, M.; Devaux, P. F.; Bodenhausen, G. *Biochimie* **1998**, *80*, 437.

10.1021/ja065461k CCC: $37.00

to give two additional, orientationally independent, chemical-shielding anisotropy (CSA) parameters for each nucleus, a potential wealth of structural information. Notwithstanding the few previous experimental[17−28] and theoretical[21−23,29−34] studies of peptides and proteins that have indicated some anisotropy dependence on the local chemical surroundings, structural variations of CSA parameters in these systems have been left largely unexplored.

Although some nonisotropic properties of the chemical-shielding tensor can be measured with solution-state NMR methods, solid-state techniques are far more suitable for ascertaining tensorial information. Solution-state NMR techniques are not limited merely by the slow tumbling of large molecular systems relative to the NMR time scale. Other difficulties include the insolubility of some macromolecules, such as membrane-associated and fibrous proteins that are aggregates existing naturally in partially ordered states. Solid-state NMR spectroscopy is one of the few techniques suitable for characterizing the structures of solids lacking long-range order, as well as amorphous systems. The pervasive need to determine the structure of biomolecules with limited order has led to the development of several solid-state NMR methods.[28,35−47] The structural interpretation of solid-state NMR experiments is not always straightforward[48−51] and often requires assumptions that cannot be validated without reliable first-principles computations of the NMR shielding tensor.

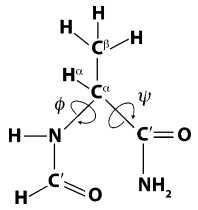

Figure 1. The For-L-Ala-NH_2 model for CSA surfaces. The dihedral angles ϕ and ψ are defined as $\phi = C'-N^H-C^\alpha-C'$ and $\psi = N^H-C^\alpha-C'-N^H$.

For proteins, solid-state NMR techniques have provided a relatively large volume of data[19] for the carbonyl carbon, C′, which, however, contains limited information on backbone dihedral angles. Fewer data are available on the shielding tensor of $^{13}C^\alpha$, which should be the best indicator of the secondary structures of proteins. The problem here is that the $^{13}C^\alpha$ tensor anisotropies are generally small and are easily obscured in magic angle spinning (MAS) measurements. In these experiments, sidebands appear around the main ICS peak as the spinning is made less rapid, and CSA parameters may be recovered from the intensities of these sidebands. However, one cannot decrease the spinning speed too much in resolving the sidebands, because this leads to widening of all the observed signals and, if the molecule contains too much labeled carbon, excessive overlap of spinning sidebands. Another hindrance for determining individual tensor components is the homonuclear coupling between C′ and C^α. Nevertheless, the development of new pulse sequences and the expensive practice of using ^{15}N- and ^{13}C-enriched samples have led to quite a number of increasingly realistic torsion-angle determinations through solid-state NMR studies.

The virtue of theoretical NMR investigations complementing experimental studies of peptides and proteins, the topic of this paper, lies not just in verifying observed results but also in providing information not directly accessible by experiments and gearing future experimental studies toward new directions. For example, experimental NMR studies have so far focused on the most populated α-helix and β-strand regions of the Ramachandran map[17−19,26,27,52] and have tried to develop relationships between ICS and CSA and the backbone dihedral angles ϕ and ψ (Figure 1) on the basis of rather limited information. Since all secondary structure types can be treated computationally with almost equal ease, the dependence of both the isotropic NMR chemical shieldings (and shifts) and the magnitude and orientation of the anisotropies of the NMR shielding tensors with respect to the dihedral angles can be studied in detail. The knowledge gained in this way should help, for example, to establish procedures able to predict the dihedral angles of peptides and proteins from the shielding tensor information provided by solid-state NMR spectroscopy.

The intimate relationship between isotropic chemical shifts and structural parameters has been investigated computationally, yielding several useful relations.[29,32,53−65] Two computational

(17) Tjandra, N.; Bax, A. *J. Am. Chem. Soc.* **1997**, *119*, 9576.
(18) Hong, M. *J. Am. Chem. Soc.* **2000**, *122*, 3762.
(19) Wei, Y. F.; Lee, D. K.; Ramamoorthy, A. *J. Am. Chem. Soc.* **2001**, *123*, 6118.
(20) Tjandra, N.; Bax, A. *J. Am. Chem. Soc.* **1997**, *119*, 8076.
(21) Heller, J.; Laws, D. D.; Tomaselli, M.; King, D. S.; Wemmer, D. E.; Pines, A.; Havlin, R. H.; Oldfield, E. *J. Am. Chem. Soc.* **1997**, *119*, 7827.
(22) Asakawa, N.; Takenoiri, M.; Sato, D.; Sakurai, M.; Inoue, Y. *Magn. Reson. Chem.* **1999**, *37*, *303.*
(23) Havlin, R. H.; Laws, D. D.; Bitter, H. M. L.; Sanders, L. K.; Sun, H. H.; Grimley, J. S.; Wemmer, D. E.; Pines, A.; Oldfield, E. *J. Am. Chem. Soc.* **2001**, *123*, 10362.
(24) Pang, Y. X.; Zuiderweg, E. R. P. *J. Am. Chem. Soc.* **2000**, *122*, 4841.
(25) Cornilescu, G.; Bax, A. *J. Am. Chem. Soc.* **2000**, *122*, 10143.
(26) Yao, X.; Yamaguchi, S.; Hong, M. *J. Biomol. NMR* **2002**, *24*, 51.
(27) Yao, X.; Hong, M. *J. Am. Chem. Soc.* **2002**, *124*, 2730.
(28) Chan, J. C. C.; Tycko, R. *J. Chem. Phys.* **2003**, *118*, 8378.
(29) Havlin, R. H.; Le, H. B.; Laws, D. D.; de Dios, A. C.; Oldfield, E. *J. Am. Chem. Soc.* **1997**, *119*, 11951.
(30) Sitkoff, D.; Case, D. A. *Prog. Nucl. Magn. Reson. Spectrosc.* **1998**, *32*, 165.
(31) Brender, J. R.; Taylor, D. M.; Ramamoorthy, A. *J. Am. Chem. Soc.* **2001**, *123*, 914.
(32) Sun, H. H.; Sanders, L. K.; Oldfield, E. *J. Am. Chem. Soc.* **2002**, *124*, 5486.
(33) Birn, J.; Poon, A.; Mao, Y.; Ramamoorthy, A. *J. Am. Chem. Soc.* **2004**, *126*, 8529.
(34) Poon, A.; Birn, J.; Ramamoorthy, A. *J. Phys. Chem. B* **2004**, *108*, 16577.
(35) Hong, M. *J. Magn. Reson.* **1999**, *139*, 389.
(36) Hong, M.; Gross, J. D.; Hu, W.; Griffin, R. G. *J. Magn. Reson.* **1998**, *135*, 169.
(37) Costa, P. R.; Gross, J. D.; Hong, M.; Griffin, R. G. *Chem. Phys. Lett.* **1997**, *280*, 95.
(38) Feng, X.; Verdegem, P. J. E.; Lee, Y. K.; Sandstrom, D.; Eden, M.; BoveeGeurts, P.; deGrip, W. J.; Lugtenburg, J.; deGroot, H. J. M.; Levitt, M. H. *J. Am. Chem. Soc.* **1997**, *119*, 6853.
(39) Hong, M.; Gross, J. D.; Griffin, R. G. *J. Phys. Chem. B* **1997**, *101*, 5869.
(40) Gregory, D. M.; Mehta, M. A.; Shiels, J. C.; Drobny, G. P. *J. Chem. Phys.* **1997**, *107*, 28.
(41) Drobny, G. P.; Long, J. R.; Karlsson, T.; Shaw, W.; Popham, J.; Oyler, N.; Bower, P.; Stringer, J.; Gregory, D.; Mehta, M.; Stayton, P. S. *Annu. Rev. Phys. Chem.* **2003**, *54*, 531.
(42) Nevzorov, A. A.; Mesleh, M. F.; Opella, S. J. *Magn. Reson. Chem.* **2004**, *42*, 162.
(43) Blanco, F. J.; Tycko, R. *J. Magn. Reson.* **2001**, *149*, 131.
(44) Rienstra, C. M.; Hohwy, M.; Mueller, L. J.; Jaroniec, C. P.; Reif, B.; Griffin, R. G. *J. Am. Chem. Soc.* **2002**, *124*, 11908.
(45) Bower, P. V.; Oyler, N.; Mehta, M. A.; Long, J. R.; Stayton, P. S.; Drobny, G. P. *J. Am. Chem. Soc.* **1999**, *121*, 8373.
(46) Gullion, T.; Schaefer, J. *J. Magn. Reson.* **1989**, *81*, 196.
(47) Wu, C. H.; Ramamoorthy, A.; Opella, S. J. *J. Magn. Reson., Ser. A* **1994**, *109*, 270.
(48) Hong, M.; Isailovic, D.; McMillan, R. A.; Conticello, V. P. *Biopolymers* **2003**, *70*, 158.
(49) Bodner, M. L.; Gabrys, C. M.; Parkanzky, P. D.; Yang, J.; Duskin, C. A.; Weliky, D. P. *Magn. Reson. Chem.* **2004**, *42*, 187.
(50) Andronesi, O. C.; Becker, S.; Seidel, K.; Heise, H.; Young, H. S.; Baldus, M. *J. Am. Chem. Soc.* **2005**, *127*, 12965.
(51) Töke, O.; Maloy, W. L.; Kim, S. J.; Blazyk, J.; Schaefer, J. *Biophys. J.* **2004**, *87*, 662.
(52) Saito, H. *Magn. Reson. Chem.* **1986**, *24*, 835.
(53) Czinki, E.; Császár, A. G.; Perczel, A. *Chem.—Eur. J.* **2003**, *9*, 1182.

routes to structure determinations from NMR chemical-shift information have been pursued. The perhaps simpler one concentrates on those limited regions of the Ramachandran surface that characterize the dominant peptide conformations. In this approach geometry optimizations are performed on all (or almost all) the possible conformers, according to a perhaps simplistic picture of a maximum of nine per residue,[66] and then NMR parameters are computed at these reference structures. This approach has been used, for example, for β-hairpin conformers[53] and dipeptide models involving diverse amino acid residues.[60−62,67] An effective utilization of the corresponding results is through the construction of multidimensional ICS−ICS plots.[53,60−62] The second route does not discriminate on the basis of conformers but uses a model peptide to define complete surfaces of NMR parameters for all relevant nuclei as a function of backbone dihedral angles.[29,32,59,63,64]

In this paper, we employ the second route, previously restricted to ICS data, to investigate the usefulness of chemical-shielding anisotropies in determining secondary structures of peptides and proteins. Most previous CSA research,[17−19,25−27,29,30,32,65,68] similar to ICS studies, has concentrated on the α-helix and β-strand regions, and the results were only used to differentiate between them. Accordingly, this paper aims at a more complete description of the dependence of CSAs on peptide backbone dihedral angles ϕ and ψ. Because CSA parameters may be defined in different ways, we also perform a mathematical analysis in search of the best carriers of structural information. In particular, new, rigorously orthogonal, and fully symmetric CSA parameters are introduced and their utility, as well as that of conventional parameters, is investigated in detail. Along the way, some deficiencies in existing measures of CSA are revealed.

2. Theoretical Methods

2.1. Computational Procedures. For exploring chemical-shielding anisotropy and its dependence on structural parameters, such as the backbone dihedral angles ϕ and ψ, we employed a simple peptide model, For-L-Ala-NH_2 (Figure 1). In order to generate CSA surfaces as a function of ϕ and ψ, a 36 × 36 grid in the [−180°, +180°] conformational space was used. This unusually dense 10° grid involves 1296 distinct structures. Because the functions to be fitted are periodic, the duplication of structures at the boundaries of the Ramachandran map is necessary, giving a total of 1369 data points. The (ϕ, ψ) dihedral angle pairs of the input structures were kept fixed while all other geometrical parameters of For-L-Ala-NH_2 were optimized at the DFT-(B3LYP)/6-31+G* level, using the program system Gaussian 98.[69]

Because the need for relatively large basis sets for NMR chemical-shielding computations is well established,[70] we used a triple-ζ plus double polarization (TZ2P)[71] basis that is especially suited for NMR shielding studies. NMR shielding tensors were computed with density functional theory for all structures resulting from the constrained optimizations on our (ϕ, ψ) grid. First, the B3LYP (Becke3−Lee−Yang−Parr)[72,73] DFT functional with the gauge-including atomic orbital (GIAO) method[74,75] was employed, as implemented in Gaussian 98.[69] Second, a simple shifting procedure was applied during the GIAO-B3LYP/TZ2P computations to improve the shielding results for non-hydrogen nuclei.[76] In this heuristic scheme, all the virtual orbital energies are uniformly increased by 32 mE_h. The shifted GIAO-B3LYP/TZ2P computations were executed within the PQS program package.[77]

2.2. Surface Fitting. To efficiently and compactly represent the computed NMR quantities as a function of the (ϕ, ψ) geometric parameters, an interpolating surface was constructed. Our previous work on ICS surfaces[59] gives a detailed description of the functions, the parameters, and the problems arising during the fitting of these complex-shaped periodic surfaces. The issues discussed there are all applicable to the present study. Here we employed the cosine series

$$a + \sum_{n=1}^{N}\left\{b_n \cos\left[n\left(\frac{\phi+\pi}{2}\right)\right] + c_n \cos\left[n\left(\frac{\psi+\pi}{2}\right)\right]\right\} + \sum_{n=1}^{N-1}\sum_{m=1}^{N-n} d_{nm} \cos\left[n\left(\frac{\phi+\pi}{2}\right)\right] \cos\left[m\left(\frac{\psi+\pi}{2}\right)\right] \quad (1)$$

with order $N = 10$ and 66 total parameters for constructing CSA surfaces. Reproduction of the computed CSA values by the fitted surfaces is good, but in terms of statistical measures not as superior as for the ICS surfaces.[59] For example, the goodness-of-fit factors, r, for the $^{13}C^{\alpha}$ surfaces were 0.99, 0.92, 0.98, and 0.92 for ρ, τ, Ω, and κ, respectively.

2.3. Analysis of B3LYP Shielding Corrections. Although DFT methods are widely used and are generally successful in predicting structures and energies of molecules, some molecular properties computed with the presently available functionals are often less accurate than expected. NMR shielding parameters of certain nuclei are in this category. Often only costly, wavefunction-based correlated methods give NMR shieldings close to experimental measurements.[78−81] DFT functionals like B3LYP[72,73] overestimate the paramagnetic component and underestimate the net shielding for nuclei in molecules containing light main-group atoms.[82] Although functionals dependent on the electron current density are formally required for an exact DFT description of magnetic properties, the observed systematic deviation of DFT shieldings from experiment is not necessarily connected with this deficiency. Inclusion of the required terms in the formalism has been found to have only a small effect for light main-group nuclei, actually increasing the net shielding.[83]

The deficiencies of commonly used functionals in NMR computations are widely assumed to arise from the inaccuracy of the virtual orbital energies. A number of attempts have been made to improve the functionals, including self-interaction corrections,[84] optimizing GGA[85]

(54) Spera, S.; Bax, A. *J. Am. Chem. Soc.* **1991**, *113*, 5490.
(55) de Dios, A. C.; Pearson, J. G.; Oldfield, E. *Science* **1993**, *260*, 1491.
(56) Jiao, D.; Barfield, M.; Hruby, V. J. *J. Am. Chem. Soc.* **1993**, *115*, 10883.
(57) Szilágyi, L. *Prog. Nucl. Magn. Reson. Spectrosc.* **1995**, *27*, 325.
(58) Iwadate, M.; Asakura, T.; Williamson, M. P. *J. Biomol. NMR* **1999**, *13*, 199.
(59) Czinki, E.; Császár, A. G. *J. Mol. Struct. (THEOCHEM)* **2004**, *675*, 107.
(60) Perczel, A.; Császár, A. G. *J. Comput. Chem.* **2000**, *21*, 882.
(61) Perczel, A.; Császár, A. G. *Chem.−Eur. J.* **2001**, *7*, 1069.
(62) Perczel, A.; Császár, A. G. *Eur. Phys. J. D* **2002**, *20*, 513.
(63) Sulzbach, H. M.; Vacek, G.; Schreiner, P. R.; Galbraith, J. M.; Schleyer, P. v. R.; Schaefer, H. F. *J. Comput. Chem.* **1997**, *18*, 126.
(64) Swalina, C. W.; Zauhar, R. J.; DeGrazia, M. J.; Moyna, G. *J. Biomol. NMR* **2001**, *21*, 49.
(65) Chekmenev, E. Y.; Xu, R. Z.; Mashuta, M. S.; Wittebort, R. J. *J. Am. Chem. Soc.* **2002**, *124*, 11894.
(66) Perczel, A.; Ángyán, J. G.; Kajtár, M.; Viviani, W.; Rivail, J. L.; Marcoccia, J. F.; Csizmadia, I. G. *J. Am. Chem. Soc.* **1991**, *113*, 6256.
(67) Császár, A. G.; Perczel, A. *Prog. Biophys. Mol. Biol.* **1999**, *71*, 243.
(68) Walling, A. E.; Pargas, R. E.; deDios, A. C. *J. Phys. Chem. A* **1997**, *101*, 7299.
(69) Frisch, M. J.; et al. *Gaussian 98*; Gaussian, Inc.: Pittsburgh, PA, 1998.
(70) Helgaker, T.; Jaszunski, M.; Ruud, K. *Chem. Rev.* **1999**, *99*, 293.
(71) Schafer, A.; Huber, C.; Ahlrichs, R. *J. Chem. Phys.* **1994**, *100*, 5829.
(72) Becke, A. D. *Phys. Rev. A* **1988**, *38*, 3098.
(73) Lee, C.; Yang, W.; Parr, R. G. *Phys. Rev. B* **1988**, *37*, 785.
(74) Ditchfield, R. *Mol. Phys.* **1974**, *27*, 789.
(75) Wolinski, K.; Hinton, J. F.; Pulay, P. *J. Am. Chem. Soc.* **1990**, *112*, 8251.
(76) Magyarfalvi, G.; Pulay, P. *J. Chem. Phys.* **2003**, *119*, 1350.
(77) *PQS*, version 3.1; Parallel Quantum Solutions: Fayetteville, Arkansas, 2004.
(78) Gauss, J.; Stanton, J. F. *J. Chem. Phys.* **1995**, *102*, 251.
(79) Gauss, J.; Stanton, J. F. *J. Chem. Phys.* **1995**, *103*, 3561.
(80) Gauss, J.; Stanton, J. F. *J. Chem. Phys.* **1996**, *104*, 2574.
(81) Gauss, J.; Stanton, J. F. *J. Chem. Phys.* **2002**, *116*, 4773.
(82) Rauhut, G.; Puyear, S.; Wolinski, K.; Pulay, P. *J. Phys. Chem.* **1996**, *100*, 6310.
(83) Lee, A. M.; Handy, N. C.; Colwell, S. M. *J. Chem. Phys.* **1995**, *103*, 10005.
(84) Hieringer, W.; Della Sala, F.; Görling, A. *Chem. Phys. Lett.* **2004**, *383*, 115.

and hybrid functionals[86] specifically for NMR shieldings, scaling down paramagnetic shieldings,[87] and using exchange-correlation potentials computed from high-level theoretical densities.[88] The first proposed scheme was simply a somewhat ad hoc formula to raise excitation energies.[89] Comparing the improvements afforded by different methods has shown that a small, uniform increase of the occupied-virtual energy gap during the shielding computations is an effective approach.[76] While the optimum values of the level shift depend slightly on the functional, the use of a constant shift greatly improves the results for nuclei in widely varied bonding situations. This uniform shift consistently brings[76] shielding tensors and ICS values significantly closer to high-level correlated wave function [CCSD(T)] results for peptide models.[53] Therefore, we adopted this shift procedure here in expectation of better shielding anisotropy predictions.

Lacking higher-level shielding predictions for comparison, it is hard to estimate how much better the shifted B3LYP shieldings are as compared to the unshifted ones. The differences in absolute shielding values are substantial for certain nuclei, especially $^{15}N^{H}$ and $^{13}C'$. For the CSA parameter ρ of section 3, we collected statistics on the deviation

$$\rho^{\mathrm{dev}}(\phi_k, \psi_k) = \left|\rho^{\mathrm{unshifted}}(\phi_k, \psi_k) - \rho^{\mathrm{shifted}}(\phi_k, \psi_k)\right| \qquad (2)$$

The deviation ranges, defined as $\max[\rho^{\mathrm{dev}}(\phi_k, \psi_k)] - \min[\rho^{\mathrm{dev}}(\phi_k, \psi_k)]$, between the shifted and unshifted surfaces are 2.96, 2.79, 2.61, 10.22, and 3.50 ppm for the nuclei $^{13}C^{\alpha}$, $^{1}H^{\alpha}$, $^{1}H^{N}$, $^{15}N^{H}$, and $^{13}C'$, respectively. By comparison, the corresponding spans of the $\rho^{\mathrm{shifted}}(\phi, \psi)$ surfaces are 38.44, 6.94, 5.92, 52.21, and 15.47 ppm, respectively. For $^{13}C^{\alpha}$, the nucleus of greatest importance for probing the Ramachandran space, the degree of parallelism between the shifted and unshifted surfaces is thus very high. None of the surfaces for the various nuclei showed significant visual changes between the two sets of shieldings. Therefore, we report data only for the shifted surfaces in this paper.

3. CSA Parameters

The full NMR shielding tensor ($\boldsymbol{\sigma}$) is nonsymmetric and of rank 2, containing 9 independent quantities [e.g., the elements of the 3 × 3 matrix of its Cartesian (x, y, z) representation]. The isotropic chemical shielding, σ_{iso}, one of the scalar invariants of the tensor, is given by $^1/_3$ of the trace of $\boldsymbol{\sigma}$:

$$\sigma_{\mathrm{iso}} = (^1/_3)\mathrm{Tr}\boldsymbol{\sigma} = (\sigma_{xx} + \sigma_{yy} + \sigma_{zz})/3 = (\sigma_1 + \sigma_2 + \sigma_3)/3 \qquad (3)$$

where σ_1, σ_2, and σ_3 are the eigenvalues of the symmetric part, $\boldsymbol{\sigma}^{\mathrm{s}}$, of the shielding tensor and the double subscripts in σ_i have been dropped in order to more clearly distinguish between principal values and general tensor elements. Experiments typically extract information about $\boldsymbol{\sigma}^{\mathrm{s}}$, which contains six independent elements, or degrees of freedom (dofs). Three of these dofs specify the orientation in space of the principal axes (eigenvectors) of $\boldsymbol{\sigma}^{\mathrm{s}}$, perhaps through three Euler angles and the corresponding direction cosine matrix, whereas the other three dofs are contained in the eigenvalues σ_1, σ_2, and σ_3. The eigenvalue space thus provides three characteristic parameters that are invariant to unitary transformations of the reference frame. Only such parameters are amenable to measurement when the orientation of the nuclei is not fixed (solution and powder spectra). The isotropic chemical shielding [σ_{iso}, eq 3], reflecting the average shielding experienced by the nuclei, leaves two dofs to describe the anisotropy of the tensor.

Some of the possible CSA parameters have been discussed previously in detail.[90,91] In NMR spectroscopy the concept of anisotropy was advanced from the theory of axially symmetric tensors, where two principal components have the same value. The so-called *anisotropy* (Δ) is the difference of the two distinct components in this generalization, $\Delta = \sigma_Z - (\sigma_X + \sigma_Y)/2 = 3(\sigma_Z - \sigma_{\mathrm{iso}})/2$, where the principal axes (X, Y, Z) of $\boldsymbol{\sigma}^{\mathrm{s}}$ are labeled according to $|\sigma_Z - \sigma_{\mathrm{iso}}| \geq |\sigma_X - \sigma_{\mathrm{iso}}| \geq |\sigma_Y - \sigma_{\mathrm{iso}}|$. Its pair, the *asymmetry* (η) was intended to show the deviation from the axially symmetric case, $\eta = (\sigma_Y - \sigma_X)/(\sigma_Z - \sigma_{\mathrm{iso}}) = 3(\sigma_Y - \sigma_X)/(2\sigma_Z - \sigma_X - \sigma_Y)$, where $0 \leq \eta \leq 1$.[90,91] In the case of an axially symmetric tensor, $\eta = 0$. The ordering of the principal components according to their separation from σ_{iso} within this convention, sometimes called the Haeberlen convention, has not always been followed strictly. This convention has several drawbacks.[90] A particular drawback, especially when anisotropy surfaces are discussed, is that (σ_X, σ_Y, σ_Z) suddenly switches from (σ_1, σ_2, σ_3) to (σ_3, σ_2, σ_1) as κ, introduced in eq 5 below, passes smoothly through 0, causing an abrupt change of sign in Δ. Thus, we avoid using $\{\Delta, \eta\}$ to represent CSA surfaces here.

The CSA parameters recommended today, sometimes called the Herzfeld−Berger convention,[90,92] are the *span* (Ω) and the *skew* (κ) of the shielding tensor

$$\Omega = \sigma_3 - \sigma_1 \qquad (\Omega \geq 0) \qquad (4)$$

and

$$\kappa = 3(\sigma_2 - \sigma_{\mathrm{iso}})/\Omega = (2\sigma_2 - \sigma_1 - \sigma_3)/\Omega \qquad (-1 \leq \kappa \leq +1) \qquad (5)$$

where the principal components (eigenvalues of $\boldsymbol{\sigma}^{\mathrm{s}}$) are labeled according to a well-established convention,[90] $\sigma_1 \leq \sigma_2 \leq \sigma_3$. One can easily derive the following inverse relationships:

$$\sigma_1 = \sigma_{\mathrm{iso}} - \Omega(\kappa + 3)/6$$
$$\sigma_2 = \sigma_{\mathrm{iso}} + \kappa\Omega/3$$
$$\sigma_3 = \sigma_{\mathrm{iso}} - \Omega(\kappa - 3)/6 \qquad (6)$$

In this paper we propose mapping CSA surfaces with a mathematically elegant pair of anisotropy parameters $\{\rho, \tau\}$ that ideally partitions CSA into physically appealing size and shape components. While these parameters are seemingly new to the NMR literature, similar quantities have appeared in other contexts.[93] Mathematically, the triplet $\{\sigma_{\mathrm{iso}}, \rho, \tau\}$ constitutes a complete set of rigorously orthogonal tensor invariants that are unaffected by unitary transformations of $\boldsymbol{\sigma}^{\mathrm{s}}$. Physically, in the space of eigenvalues (σ_X, σ_Y, σ_Z), the isosurfaces of σ_{iso} are planes with $\mathbf{m} = (1,1,1)/\sqrt{3}$ as a common normal vector, those of ρ are cylinders with a common axis $\mathbf{w}$ that passes through the origin and is directed along $\mathbf{m}$, and those of τ are half-planes containing and pivoting about $\mathbf{w}$. In essence, $\{\sigma_{\mathrm{iso}}, \rho, \tau\}$ forms a tilted, cylindrical coordinate system in eigenvalue space

(85) Keal, T. W.; Tozer, D. J. *J. Chem. Phys.* **2003**, *119*, 3015.
(86) Wilson, P. J.; Amos, R. D.; Handy, N. C. *Chem. Phys. Lett.* **1999**, *312*, 475.
(87) Chesnut, D. B. *Chem. Phys. Lett.* **2003**, *380*, 251.
(88) Wilson, P. J.; Tozer, D. J. *Chem. Phys. Lett.* **2001**, *337*, 341.
(89) Malkin, V. G.; Malkina, O. L.; Casida, M. E.; Salahub, D. R. *J. Am. Chem. Soc.* **1994**, *116*, 5898.
(90) Mason, J. *Solid State Nucl. Magn. Reson.* **1993**, *2*, 285.
(91) Jameson, C. J. *Solid State Nucl. Magn. Reson.* **1998**, *11*, 265.
(92) Herzfeld, J.; Berger, A. E. *J. Chem. Phys.* **1980**, *73*, 6021.
(93) Criscione, J. C.; Humphrey, J. D.; Douglas, A. S.; Hunter, W. C. *J. Mech. Phys. Solids* **2000**, *48*, 2445.

corresponding, apart from a numerical factor, to the (radial, azimuthal, axial) geometric variables customarily labeled as (r, ϕ, z). Accordingly, ρ and τ describe the magnitude (norm) and orientation (mode) of the anisotropy, respectively. In detail

$$\rho = \sqrt{[(\sigma_1 - \sigma_2)^2 + (\sigma_1 - \sigma_3)^2 + (\sigma_2 - \sigma_3)^2]/2} = \sqrt{3\mathrm{Tr}(\tilde{\boldsymbol{\sigma}}\tilde{\boldsymbol{\sigma}}^T)/2} \quad (7)$$

and

$$3\tau = k\pi + (-1)^{k+1} \arcsin[\mathrm{mode}(\tilde{\boldsymbol{\sigma}})] \quad (k = 0, \pm1, \pm2, \pm3) \quad (8)$$

where $\tilde{\boldsymbol{\sigma}} = \boldsymbol{\sigma}^s - \sigma_{iso}\mathbf{I}_3$ is the anisotropic part of the symmetric shielding tensor, $\mathbf{I}_3$ is the 3×3 unit matrix, $\mathrm{norm}(\tilde{\boldsymbol{\sigma}}) = \sqrt{\mathrm{Tr}(\tilde{\boldsymbol{\sigma}}\tilde{\boldsymbol{\sigma}}^T)}$ is the Frobenius norm, and

$$\mathrm{mode}(\tilde{\boldsymbol{\sigma}}) = \frac{1}{2\rho^3}(2\sigma_1 - \sigma_2 - \sigma_3)(2\sigma_2 - \sigma_1 - \sigma_3)(2\sigma_3 - \sigma_1 - \sigma_2) = 3\sqrt{6}\,\det\left[\frac{\tilde{\boldsymbol{\sigma}}}{\mathrm{norm}(\tilde{\boldsymbol{\sigma}})}\right] \quad (9)$$

For the usual convention $\sigma_1 \le \sigma_2 \le \sigma_3$, we have $k = 0$ in eq 8 and $\tau \in [-\pi/6, +\pi/6]$. The $(-\pi/6, +\pi/6)$ limits of τ correspond to the (oblate, prolate) axial tensor limits. As such, τ can also be viewed as a measure of the *shape* of the anisotropy.

Both $\mathrm{norm}(\tilde{\boldsymbol{\sigma}})$ and $\mathrm{mode}(\tilde{\boldsymbol{\sigma}})$ can be computed directly from the $\boldsymbol{\sigma}^s$ tensor elements without diagonalization and are completely symmetric with respect to the eigenvalues, as clearly seen from eqs 7 and 9. The $\{\rho, \tau\}$ anisotropy variables have a remarkably simple relationship to the conventional $\{\Omega, \kappa\}$ set:

$$(\Omega, \kappa) = \left(\frac{2}{\sqrt{3}}\rho\cos\tau, \quad \sqrt{3}\tan\tau\right) \quad (10)$$

Note that for an axially symmetric tensor the norm, ρ, becomes identical to the span, Ω, explaining the normalization factor in eq 7. The eigenvalues of $\boldsymbol{\sigma}^s$ can also be recovered trivially from $\{\sigma_{iso}, \rho, \tau\}$ by means of

$$(\sigma_1, \sigma_2, \sigma_3) = \sigma_{iso}(1, 1, 1) + \frac{\rho\cos\tau}{\sqrt{3}}(-1, 0, 1) + \frac{\rho\sin\tau}{3}(-1, 2, -1) \quad (11)$$

Finally, $\{\rho, \tau\}$ can be evaluated from $\{\Omega, \kappa\}$ as

$$(\rho, \tau) = \left(\frac{\Omega}{2}\sqrt{3 + \kappa^2}, \quad \frac{1}{3}\arcsin\left[\frac{\kappa(9 - \kappa^2)}{(3 + \kappa^2)^{3/2}}\right]\right) \quad (12)$$

The simplicity of eqs 10 and 12 allows facile interconversion of CSA parameters from different studies and maintains a clear connection of $\{\rho, \tau\}$ to experimental observables. Investigation of $\{\rho, \tau\}$ is warranted because this physically appealing dissection of CSA information might provide enhanced capabilities for distinguishing secondary structures of peptides and proteins.

The $\boldsymbol{\sigma}^s$ tensor of a nucleus carries information not only about the magnitude of the chemical shielding and its different partitions but also about its orientation with respect to the principal axes of the molecule. The experimental determination of tensor orientation information for nuclei in peptides and proteins has many limitations,[27] and thus far dependable data are scarce. The tensor orientation with respect to the molecular frame can be expressed in various ways. One possibility involves the three Euler angles or the direction cosines relating the principal axes of the shielding tensor of a given nucleus to the principal axes of the moment of inertia of the molecule.[26,31] This choice and its consequences are not investigated in this paper.

Another possibility of specifying tensor orientation involves angles between certain σ_i axes and a chosen internuclear vector.[29,33,34] A related commonly used definition is

$$\Delta\sigma^* = \sigma_{orth} - \sigma_{par} \quad (13)$$

where σ_{par} is the shielding in a particular direction in the molecular frame and σ_{orth} is the average of the two orthogonal components. Instead of transforming $\boldsymbol{\sigma}^s$ to a new reference frame, $\Delta\sigma^*$ is often computed with (σ_{par}, σ_{orth}) set to the principal values whose eigenvectors are most closely (parallel, perpendicular) to the chosen internuclear axis. In this case, the definition of $\Delta\sigma^*$ clearly resembles that of the anisotropy Δ. In a few instances $\Delta\sigma^*$ has been determined from solution-state NMR relaxation measurements. For example, in the case of C^α, $\Delta\sigma^*$ in relation to the $C^\alpha{-}H^\alpha$ bond is often measured following ref 17. The use of $\Delta\sigma^*(\phi, \psi)$ CSA surfaces for predicting secondary structures of proteins is included in the investigations of this paper.

4. Secondary Structures from CSA Parameters

Contradictory statements exist in the literature about the utility and predictive power of the most commonly employed nondirectional anisotropy parameter, Ω, the tensor span. All studies on the conformational dependence of ICS and CSA data, in accord with simple chemical principles, suggest that the $^{13}C^\alpha$ nucleus holds the greatest promise in localizing (ϕ, ψ) effects. One of the latest investigations[32] states that only β-branched (β-disubstituted) amino acids have a large span difference between α-helical and β-strand conformers for $^{13}C^\alpha$.

In this study, entire $\Omega(\phi, \psi)$, $\kappa(\phi, \psi)$, $\rho(\phi, \psi)$, and $\tau(\phi, \psi)$ surfaces have been generated for the nuclei of the model peptide For-L-Ala-NH_2 for the following reasons: (a) there are considerable (ϕ, ψ) variations among experimental α-helix and β-strand structures; (b) anisotropy data from regions of the Ramachandran map other than α-helix and β-strand are almost never available from experimental studies; and (c) our model surfaces may find future use in conformational predictions and structural refinements. For the $^{13}C^\alpha$ nucleus we found striking resemblance of the $\rho(\phi, \psi)$ and $\Omega(\phi, \psi)$ surfaces, as well as the $\tau(\phi, \psi)$ and $\kappa(\phi, \psi)$ surfaces, each pair being indistinguishable by the eye. This observation is in accord with eq 12, after noting that the $^{13}C^\alpha$ tensor is far from being axially symmetric over the Ramachandran surface, that is, κ^2 is small compared to 3. However, the similarity of the (ρ, Ω) and (τ, κ) pairs of surfaces should not be regarded as a general occurrence, because the limit $\kappa^2 \ll 3$ may not be realized for other nuclei and in other environments.

The representative $\rho(\phi, \psi)$ and $\tau(\phi, \psi)$ surfaces for the $^{13}C^\alpha$ nucleus are displayed in Figure 2. Both surfaces are highly structured and contain several maxima and minima. An ideal, unambiguous situation for the use of CSA data would occur if

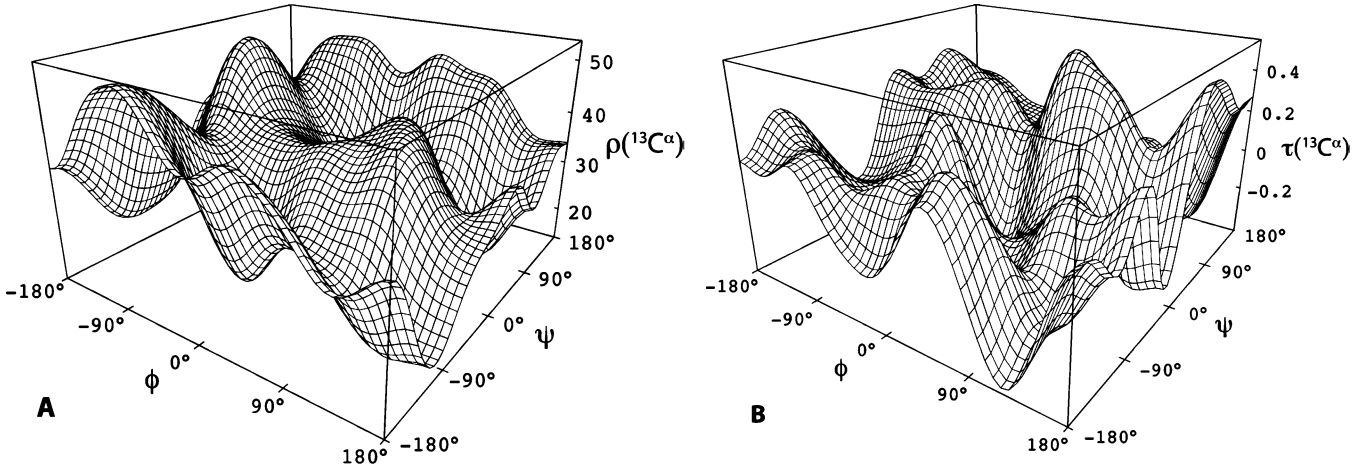

Figure 2. Complex structure of the $\rho(\phi, \psi)$ (panel A) and $\tau(\phi, \psi)$ (panel B) surfaces of the $^{13}C^{\alpha}$ nucleus of For-L-Ala-NH_2. For both panels A and B, a 10th-order cosine fitting [eq 1] was employed for all data points computed by the shifted DFT method. Units of ρ and τ are ppm and rad, respectively.

Table 1. Comparison of Experimental and Theoretical ρ Values for the C^{α} Nucleus of Alanine Residues for α-Helical and β-Strand Conformers

	experimental					
	compound	ϕ (deg)	ψ (deg)	ref	ρ^a	theoretical ρ^b
α-helix	Poly-L-Ala	average for α-helix		19	31.25	*c*
	Boc-V*AL-Aib-VAL-OMe(1)[d]	−65.4	−44.5	23	35.78	33.95
		−61.0	−44.4			33.54
	Boc-V*AL-Aib-VAL-OMe(2)[d]	−76.0	−44.0	23	35.00	35.03
	poly-Ala film	−57.4	−47.5	22		32.77
	G*AV	−68.7	−38.1	23	44.71	34.83
	G*AL	−65.7	−40.0	26	30.35	34.42
β-strand	A*AA mol A	−143.4	160.2	23	41.14	41.38
	A*AA-hemihyd	−145.7	145.5	23	41.54	38.28
		−156.2	149.9			36.23
	stretched poly-Ala film (I)	−138.8	134.7	22	25.93	38.39
	stretched poly-Ala film (II)				22.65	
	Poly-L-Ala	average for β-strand		19	27.91	*c*

[a] Chemical-shielding tensor components available in the references given were used to compute ρ via eq 7. [b] Determined from the fitted Ramachandran $\rho(\phi, \psi)$ surface. [c] For comparing to experimental α-helix and β-strand values when no "exact" (ϕ, ψ) dihedral angles are available, one can take the computed CSA values at (−60, −40) and (−120, 120) for helical and β-strand conformers, respectively. These are ρ (−60, −40) = 34.04 ppm and ρ (−120, 120) = 39.80 ppm. Havlin et al.[29] have reported computed values only at the grid point (−60, −45) in the case of α-helix; their corresponding ρ values are 25.9 ppm for helical and 24.9 ppm for β-strand conformers. [d] Aib = α-aminoisobutyric acid; (1) crystallized from MeOH−H_2O; (2) crystallized from DMSO-2-propanol.

dominant, highest peaks and/or lowest wells on the surfaces were associated with major secondary structures. In actuality, there is considerable overlap of ρ and τ values corresponding to the α-helix $[(\phi, \psi) \approx (-50°, -40°)]$ and β-strand $[(\phi, \psi) \approx (-130°, 130°)]$ conformational regions, and none of the CSA parameters individually is able to distinguish clearly between these two major secondary structures. The related difficulty in conformational predictions based on experimental information[19,22,23,26,29] is seen in the overlapping ρ data collected in Table 1.

A way forward is to correlate CSA pairs like $\{\rho, \tau\}$ or $\{\Omega, \kappa\}$ that contain the complete anisotropy information about the shielding tensor of a given nucleus. Panel A of Figure 3 shows a two-dimensional (2D) ρ versus τ correlation plot constructed from our data for the C^{α} nucleus. The corresponding graph of Ω versus κ is very similar in all respects. In the ρ versus τ plot, the loci of points from the most populated four regions of the Ramachandran surface, α-helix, β-strand, left-handed α-helix, and polyproline II, are clearly disjointed. This clustering effect seems to provide a simple and useful method for secondary structure determination on the basis of direct use of experimental CSA information. A more sophisticated graph is obtained when a three-dimensional (3D) correlation plot, σ_{iso} versus ρ versus τ is prepared for the C^{α} nucleus (panel B of Figure 3). The clustering of the different secondary structures is even more evident on this 3D graph than on its 2D analogue.

To the best of our knowledge there are no experimental studies reporting $^1H^{\alpha}$ and $^1H^N$ chemical-shielding tensor principal components. Consequently, we cannot extract CSA parameters from experimental information and compare them to our computed results. There are one or two shielding tensor principal component measurements[24,31,33] for $^{15}N^H$ and $^{13}C'$, but comparisons based on a maximum of two data points would not be very meaningful. Therefore, our $\rho(\phi, \psi)$, $\tau(\phi, \psi)$, and ρ versus τ plots for these nuclei are not shown here.

The 2D and 3D correlation plots for $^{13}C^{\alpha}$ of For-L-Ala-NH_2, with a clear clustering of the secondary structure elements, seem to offer useful tools for secondary structure predictions for proteins. Although these results were obtained for a simple model compound, it is expected that they hold true not only for Ala residues in proteins but also for most other residues. We hope that the present study will prompt experimental

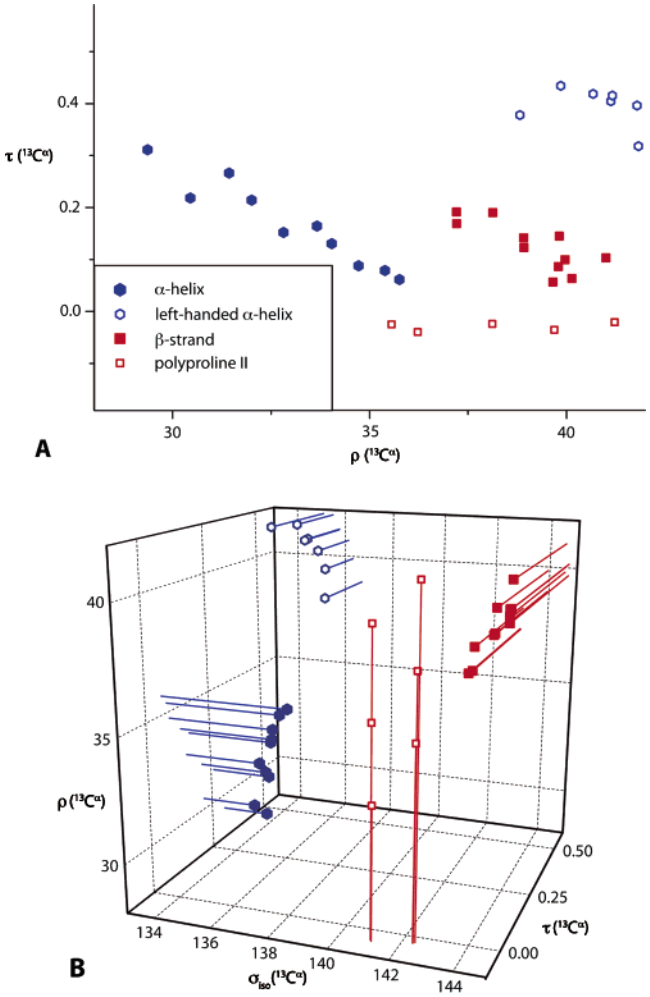

Figure 3. The ρ vs τ (panel A) and σ_{iso} vs τ vs ρ (panel B) correlation plots for the $^{13}C^{\alpha}$ nucleus of For-L-Ala-NH_2 using (ϕ, ψ) values (see Figure 4) in each region characterizing the four major secondary structure elements. Units of σ_{iso}, τ, and ρ are ppm, rad, and ppm, respectively.

measurements of much-needed data to investigate the observed relationships further.

An alternative to these simple correlation plots for secondary structure determinations is the *Z*-surface probability weighting technique first introduced for NMR chemical shifts by Oldfield and co-workers.[94] This method could be adapted to include empirical NMR anisotropy data of various nuclei in protein structure refinements by constructing probability functions from computed CSA (ϕ, ψ) surfaces. While the shape of the surfaces and the relative CSAs computed in this study should be correct, empirical scaling may be needed to ensure sufficient absolute accuracy for quantitative *Z*-surface refinements.

The orientation of the $^{13}C^{\alpha}$ tensor is greatly affected by the backbone dihedral angles.[17,18,23,29,30,32,68] Our theoretical data provide detailed assessment of this phenomenon. Figure 4 tracks the variation of the principal component of the $^{13}C^{\alpha}$ chemical-shielding tensor that is most closely directed along the $C^{\alpha}-H^{\alpha}$ bond vector. The white regions of the plot show where the axis corresponding to σ_1 has the smallest inclination with respect to the $C^{\alpha}-H^{\alpha}$ bond. The gray and black areas reveal that the σ_1 axis may tilt away so that σ_2 or even σ_3 most closely aligns with the $C^{\alpha}-H^{\alpha}$ bond vector. Note especially that the prevalent α-helix region has σ_2 closest to the $C^{\alpha}-H^{\alpha}$ direction. Consequently, the usual assumption[18] of computing $\Delta\sigma^*$ values for $^{13}C^{\alpha}$ by setting $\sigma_{par} = \sigma_1$ in eq 13 is not valid over the whole Ramachandran surface. As Figure 5 and Table 2 show, this problem is unique to C^{α}, as for the other nuclei of interest ($^{15}N^{H}$, $^{1}H^{N}$, and C′), there is always a single axis parallel to a naturally chosen internuclear vector over the whole Ramachandran surface, in accord with literature results.[25,39]

We constructed $\Delta\sigma^*(\phi, \psi)$ surfaces for $^{13}C^{\alpha}$, always taking the eigenvalue of the principal axis most closely aligned with $C^{\alpha}-H^{\alpha}$ as σ_{par} and the average magnitude of the other two components as σ_{orth}. This customary approach does not involve transformation of $\boldsymbol{\sigma}^{S}$ to the internuclear axis system. The results in Table 3 seem to suggest that $\Delta\sigma^*$ of $^{13}C^{\alpha}$ is suitable in itself for discriminating between the α-helical and β-strand secondary structures, since there is a large difference in the range of $\Delta\sigma^*$ values of these conformations. The $\Delta\sigma^*$ value is large for the β-strand region and almost zero for the α-helical region, as first shown by Tjandra and Bax.[17] In Table 3 there are some sizable variations in $\Delta\sigma^*$ values from different models, methods, and measurements. For example, magic-angle sample-spinning solid-state NMR measurements[23] give $\Delta\sigma^* = 28.5$ ppm for compound A*AA mol A, whereas GIAO Hartree-Fock computations[23] on the For-L-Ala-NH_2 fragment produce $\Delta\sigma^* = 23.0$ ppm, and our shifted GIAO-B3LYP/TZ2P model surfaces yield $\Delta\sigma^* = 38.0$ ppm. Nonetheless, the α-helix and β-strand data do not interlace. Unfortunately, as shown in ref 68 and more explicitly in Figure 4, the main reason behind this seemingly useful[17] distinction is that for $^{13}C^{\alpha}$ in the β-strand region $\sigma_{par} = \sigma_1$, while for a large part of the α-helical region $\sigma_{par} = \sigma_2$. In the latter case the axially nonsymmetric tensor results in $\Delta\sigma^*$ values close to zero. Consequently, although $\Delta\sigma^*$ appears to be quite suitable for discriminating between α-helix and β-strand secondary structures, the information obtained this way should be used with some caution, because when one ends up in a region of the α-helix where $\sigma_{par} = \sigma_1$ or σ_3, this discrimination will clearly break down.

Because the whole $\Delta\sigma^*(\phi, \psi)$ surface is available computationally as a source of useful information, we can consider regions other than α-helix and β-strand as well. For the α_D (left-handed α-helix) region of the $\Delta\sigma^*$ surface of $^{13}C^{\alpha}$, the $\Delta\sigma^*$ values coincide with those of the β-strand region. Therefore, these regions cannot be discriminated on the basis of $\Delta\sigma^*$ values. The α_D and α_L regions seem to be characterized by sufficiently different $\Delta\sigma^*$ values. For the polyproline II structure, the $\Delta\sigma^*(^{13}C^{\alpha})$ values partly overlap with those of the β-strand. Since these two regions are neighbors in the Ramachandran map (Figure 4), this behavior is not unexpected.

Multinuclear correlation plots of CSA data also appear to be effective tools for structure studies. Figure 6 presents $\rho(^{1}H^{\alpha})$ versus $\rho(^{13}C^{\alpha})$ and $\Delta\sigma^*(^{1}H^{\alpha})$ versus $\Delta\sigma^*(^{13}C^{\alpha})$ correlation plots. The four common secondary structural elements are generally distinguishable by clustering in these 2D layouts. However, in the $\rho(^{1}H^{\alpha})$ versus $\rho(^{13}C^{\alpha})$ graph, the β-strand and polyproline II regions are intertwined, an ambiguity not observed in the mononuclear 2D and 3D correlations in Figure 3. Further theoretical and experimental explorations are warranted to reveal which multinuclear correlations are most likely to yield clear signatures of secondary structures.

(94) Le, H. B.; Pearson, J. G.; de Dios, A. C.; Oldfield, E. *J. Am. Chem. Soc.* **1995**, *117*, 3800.

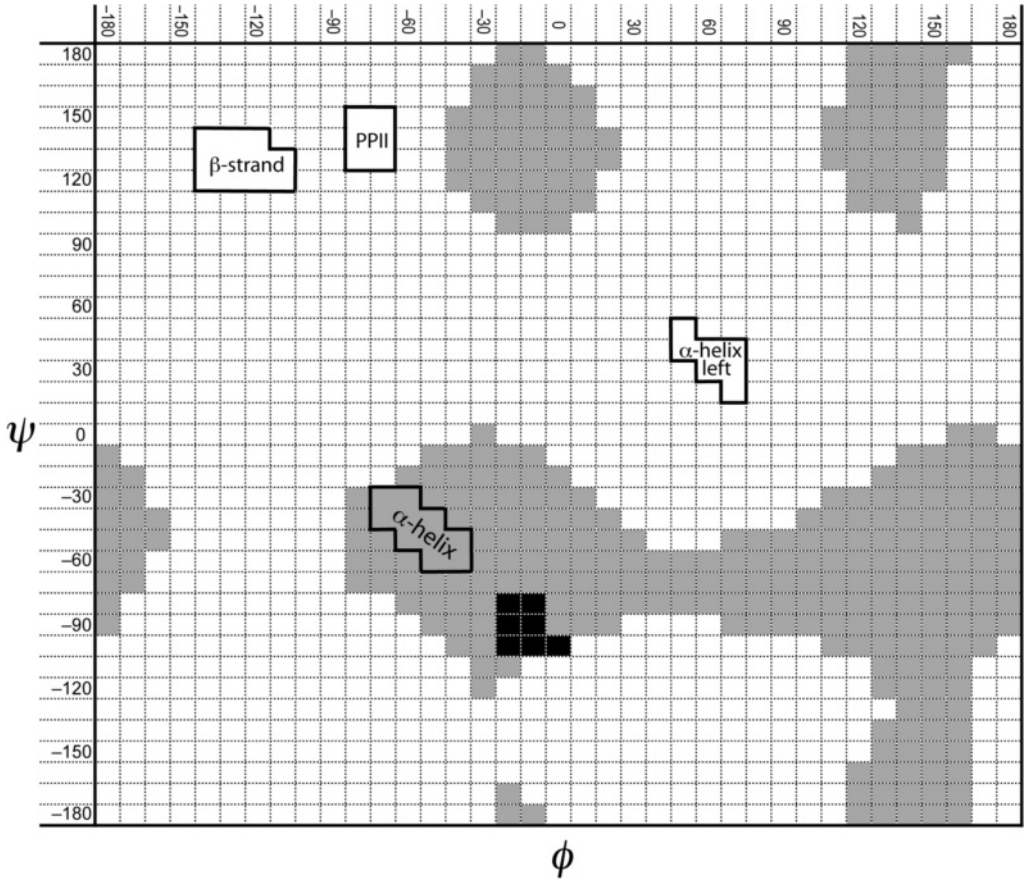

Figure 4. Variation over the Ramachandran surface of the principal component of the $^{13}C^{\alpha}$ chemical-shielding tensor having the smallest incline with respect to the $C^{\alpha}-H^{\alpha}$ bond vector. The white areas correspond to σ_1, the gray to σ_2, and the black to σ_3. The enclosed areas correspond roughly to β-strand ($\phi \approx -130°$, $\psi \approx 130°$), polyproline II ($\phi \approx -70°$, $\psi \approx 140°$), α-helix ($\phi \approx -50°$, $\psi \approx -40°$), and left-handed α-helix ($\phi \approx 60°$, $\psi \approx 40°$) regions.

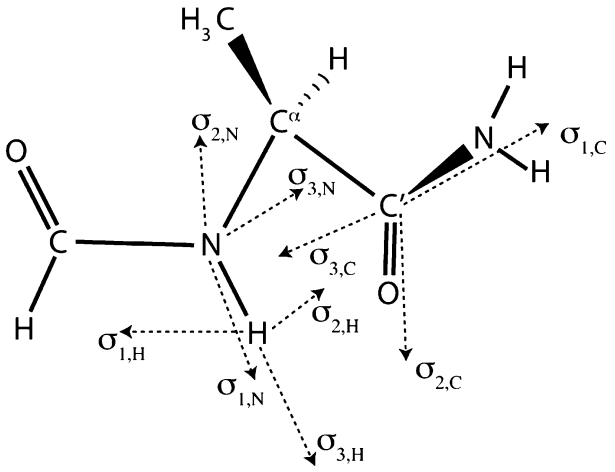

Figure 5. General orientation of principal axes of the N^H, H^N, and C′ chemical-shielding tensors.

Table 2. Statistical Data for Angles of Inclination (deg) between Selected Principal Axes of $^1H^N$, $^{15}N^H$, and $^{13}C'$ Shielding Tensors and Adjacent Bond Vectors.

	full surface	α-helix	β-strand
	$^1H^N$ (N−H and σ_3)		
average	13.90	13.59	12.27
std dev	5.29	3.52	5.12
max	34.07	20.19	21.68
min	0.25	8.96	0.25
	$^{15}N^H$ (N−H and σ_1)		
average	12.79	12.61	16.85
std dev	3.56	0.88	2.03
max	21.64	14.25	20.72
min	4.59	11.21	12.17
	C′ (C═O and σ_2)		
average	3.65	2.39	2.69
std dev	2.22	0.82	0.92
max	10.83	5.32	4.12
min	0.14	0.73	0.46

5. Summary

An appealing pair of parameters has been introduced to describe the size and shape of the NMR chemical-shielding anisotropy: $\rho = 2^{-1/2}[(\sigma_1 - \sigma_2)^2 + (\sigma_1 - \sigma_3)^2 + (\sigma_2 - \sigma_3)^2]^{1/2}$ and $\tau = -1/3 \arcsin[(2\sigma_1 - \sigma_2 - \sigma_3)(2\sigma_2 - \sigma_1 - \sigma_3)(2\sigma_3 - \sigma_1 - \sigma_2)/(2\rho^3)]$, where the σ_i are the eigenvalues of the symmetric part ($\boldsymbol{\sigma}^s$) of the shielding tensor. Mathematically, the triplet $\{\sigma_{iso}, \rho, \tau\}$ is a complete set of rigorously orthogonal tensor invariants that are unaffected by molecular rotations. These parameters are recommended for both their elegance and practicality in cataloging and comparing NMR chemical-shielding information. Traditional, nondirectional CSA parameters, like span (Ω), skew (κ), anisotropy (Δ), and asymmetry (η) are readily computed from ρ and τ, and vice versa.

The dependence of CSA on secondary structure has been investigated by computing ρ and τ surfaces on a dense grid in the Ramachandran space of backbone torsional angles ϕ and ψ for a model peptide, For-L-Ala-NH_2. The TZ2P DFT(B3LYP)-GIAO level of theory was employed using two formalisms, a traditional (unshifted) one and an improved (shifted) scheme in which the virtual orbital energies were uniformly increased

Table 3. $\Delta\sigma^*$ of $^{13}C^{\alpha}$ for α-Helical and β-Strand Regions

	other studies (experimental or theoretical)						
					Δσ*/ppm		
	compound	φ (deg)	ψ (deg)	ref	exptl	theoret	present theoretical[a] Δσ* /ppm
α-helix	ubiquitin and CaM/M13	average for α-helix		17	6.1 ± 4.9		*b*
	For-Aaa-Aaa-NH_2	−60	−60	68		0 to −11	−2.0
	Alanine dipeptide	around (−60, −60) on their surface		30		≤0	*b*
	Boc-V*AL-Aib-VAL- OMe(1)[c]	−65.4	−44.5	23	1.5	2.5	3.4
		−61.0	−44.4				0.8
	Boc-V*AL-Aib-VAL- OMe(2)[c]	−76.0	−44.0	23	4.4	7.6	10.3
	G*AV	−68.7	−38.1	23	9.2	6.6	7.8
β-strand	ubiquitin and CaM/M13	average for β-strand		17	27.1 ± 4.3		*e*
	For-Aaa−Aaa-NH_2	−120	−120	68		29−37[d]	36.5
	Alanine dipeptide	around (−120, −120) on their surface		30		∼30	*e*
	A*AA mol A	−143.4	160.2	23	28.5	23.0	38.0
	A*AA-hemihyd	−145.7	145.5	23	29.1	22.0	34.9
		−156.2	149.9				33.6

[a] $\Delta\sigma^*$ values determined from the shifted TZ2P B3LYP $\Delta\sigma^*(\phi, \psi)$ surfaces (see text). [b] No (ϕ, ψ) dihedral angles are given in the literature. For comparison, the computed $\Delta\sigma^*$ values around (−60, −60) are in the range −4 to +2 ppm. [c] Aib = α-aminoisobutyric acid; (1) crystallized from MeOH−H_2O; (2) crystallized from DMSO-2-propanol. [d] Except for Asn and His. [e] No (ϕ, ψ) dihedral angles are given in the literature. For comparison, the computed $\Delta\sigma^*$ values around (−120, 120) are ∼36 ppm.

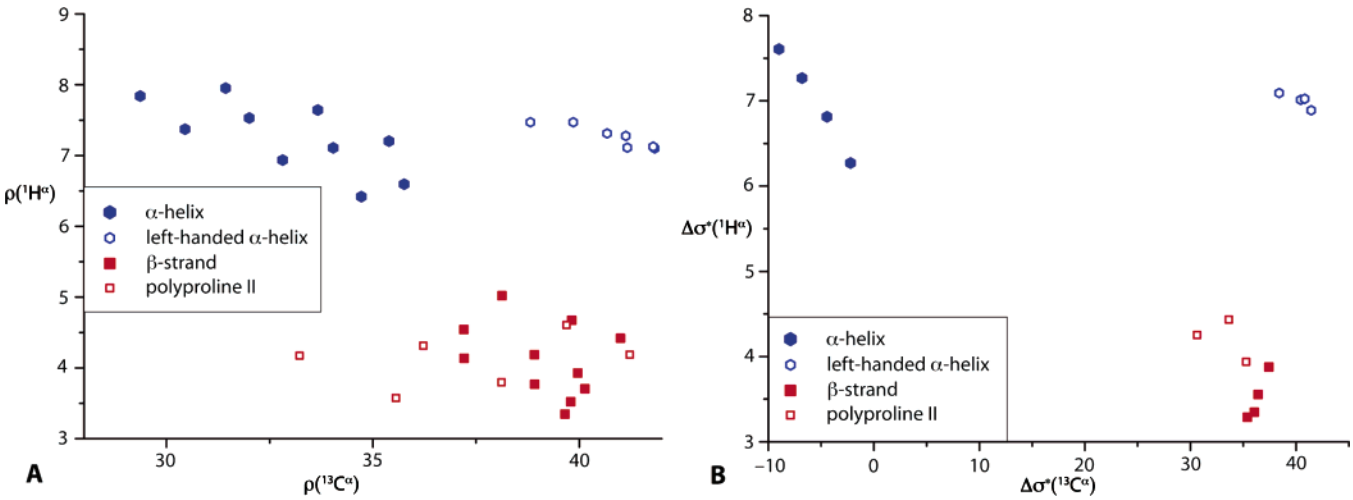

Figure 6. $\rho(^{13}C^{\alpha}) - \rho(^{1}H^{\alpha})$ (panel A) and $\Delta\sigma^*(^{13}C^{\alpha}) - \Delta\sigma^*(^{1}H^{\alpha})$ (panel B) correlation plots using $\phi - \psi$ values indicated in Figure 4 as enclosed areas. All parameters in ppm.

by 32 mE_h. None of the surfaces exhibited any qualitative changes between the unshifted and shifted computations, supporting the overall utility and relative accuracy of the results. The 10th-order cosine series of eq 1 was used to satisfactorily fit the CSA surfaces. At least some of the surfaces generated for For-L-Ala-NH_2 are expected to find further use when more experimental CSA data on proteins become available.

The computed CSA surfaces are highly structured, and the *individual* anisotropy parameters do not unambiguously distinguish between the four major secondary structure types, α-helix, β-strand, left-handed α-helix (α_D), and polyproline II. However, when the complete anisotropy information is employed in ρ versus τ (or Ω versus κ) correlation plots for $^{13}C^{\alpha}$, the nucleus most suitable for probing backbone torsional angles, all the major secondary structures stand out as clusters in distinctively different regions of the 2D correlation plots. A similar three-dimensional correlation plot, $\sigma_{iso}(^{13}C^{\alpha})$ versus $\rho(^{13}C^{\alpha})$ versus $\tau(^{13}C^{\alpha})$, seems to be especially useful for elucidating secondary structures of proteins with measured CSA data.

Experimental studies have suggested that $\Delta\sigma^*$ of $^{13}C^{\alpha}$ is a useful tool for protein backbone conformation predictions. The $\Delta\sigma^*(\phi, \psi)$ surface of $^{13}C^{\alpha}$ mapped out in this study reveals that the angle of inclination between the principal axis corresponding to σ_1 and the $C^{\alpha}-H^{\alpha}$ bond vector varies considerably with ϕ and ψ. The σ_1 axis may tilt completely away from the $C^{\alpha}-H^{\alpha}$ bond and become almost orthogonal to it, while the axis of σ_2 or even σ_3 may become most nearly parallel to $C^{\alpha}-H^{\alpha}$. Therefore, the main reason behind the seemingly useful $\Delta\sigma^*$ discrimination between α-helix and β-strand secondary structures is that for $^{13}C^{\alpha}$ in the β-strand region $\sigma_{par} = \sigma_1$, while for a large part of the α-helical region $\sigma_{par} = \sigma_2$. Consequently, $\Delta\sigma^*(^{13}C^{\alpha})$ information should be used with caution because axis switching may suddenly occur in traversing the Ramachandran surface.

Analysis of the massive set of CSA data computed here for the simple model peptide For-L-Ala-NH_2 has revealed some promising relationships that could be generally exploited in determining secondary structures of proteins. The key question is the extent to which CSA is governed by the local chemical environment, thus allowing the construction of semiuniversal functions, particularly for $^{13}C^{\alpha}$, describing the dependence of the shielding anisotropy on the backbone torsional angles ϕ and

ψ. Such functions, as developed here, could allow measured CSA data to be included in predicate least-squares (or *Z*-surface[94]) refinements of protein secondary structures. Toward this goal, it would be fortunate if CSA is less susceptible than ICS to nonlocal effects, e.g., aromatic ring currents. Several research directions are now warranted. First, DFT methods could be used to generate CSA surfaces for larger model peptides, including various short sequences of amino acids, as well as residues with sizable side chains. Second, the calibration of DFT predictions could be improved by the arduous application of high levels of theory to larger benchmark systems. Finally, and most importantly, we hope that the present study will stimulate experimental NMR measurements of much-needed anisotropy data to further investigate the relationships observed here between CSA parameters and secondary structure.

Acknowledgment. The work performed in Budapest received partial support from the Hungarian Scientific Research Fund, OTKA, through Grants T047185 and F33002. Collaborations between Budapest and Athens, GA, were supported by an NSF-MTA-OTKA travel grant (Grant INT-0312355). Discussions with Dr. O. Töke concerning solid-state NMR spectroscopy are gratefully acknowledged. P.R.S. thanks Dr. H. Hausmann for fruitful discussions.

Supporting Information Available: Complete ref 69. This material is available free of charge via the Internet at http://pubs.acs.org.

JA065461K